New York University

Department of Mechanical and Aerospace Engineering

Evaporative Cooling System for Photovoltaic Panels

Mechatronics

Rajat Gupta
Eva Langenbrunner
Berinay Demirci

Instructor: Prof. Nicholas Chbat

December 20, 2025

Table of Contents

Abstract - This project investigates the use of evaporative cooling to mitigate temperature-induced efficiency losses in photovoltaic panels. A closed-loop, Arduino based control system was developed to monitor panel temperature, actuate an ultrasonic misting device, and estimate electrical power output under controlled indoor irradiance conditions. Artificial illumination was used to independently reproduce the thermal and electrical effects of solar exposure, enabling repeatable experimentation. A first-order thermal model of the panel, actuator, and sensor was derived and implemented in Simulink, and a second-order controller with relay-based hysteresis was designed to regulate panel temperature. Experimental results demonstrate that evaporative cooling successfully limits panel temperature rise and reduces power degradation compared to uncooled operation. While the system exhibits a net energy cost at small scale, the results validate the effectiveness of thermal regulation and provide a control-oriented framework for future high-fidelity and large-scale implementations.

1 Introduction

Photovoltaic panel efficiency is strongly dependent on operating temperature, with electrical output decreasing as panel temperature rises above nominal conditions. In real outdoor environments, solar panels are exposed to continuous thermal loading from solar irradiance, elevated ambient temperatures, and limited convective cooling, leading to measurable performance degradation. As a result, thermal effects cannot be neglected in photovoltaic system design.

Evaporative cooling offers a simple and potentially effective approach for reducing panel temperature by leveraging latent heat transfer during water evaporation. However, the effectiveness of such systems depends not only on the cooling mechanism itself, but also on how and when cooling is applied. Continuous or uncontrolled cooling can lead to unnecessary energy and water consumption, reducing overall system efficiency.

This project approaches photovoltaic cooling as a control and system-level problem rather than a purely materials-based solution. A closed-loop control system was developed to actively regulate panel temperature using evaporative misting driven by real-time temperature feedback. Due to practical constraints on outdoor testing, an indoor experimental setup was designed that separates thermal loading from electrical irradiance using independent light sources. Mathematical models for the panel, actuator, and sensor were derived to support simulation, controller design, and experimental validation.

The primary objectives of this project are to design and implement a closed-loop evaporative cooling system for a PV panel, model the dominant thermal dynamics for control-oriented analysis, and experimentally evaluate the effect of controlled cooling on panel temperature and power output.

2 Hardware Architecture

This section presents a detailed breakdown of the system hardware, including actuator wiring, sensing components, and their integration with the Arduino I/O interface. It explains how temperature sensing, mist actuation, and solar power measurement were electrically and logically connected, and outlines the design decisions that guided the final hardware architecture. The discussion follows the progression from component selection through wiring configuration to reliable microcontroller communication, providing insight into the engineering rationale behind the final implementation.

2.1 Mister and Temperature System

The mister and temperature sensing system is shown in Figure 1 and can be divided into two subsystems. The first subsystem measures the solar panel temperature using a 10 $k\Omega$ precision epoxy thermistor (3950 NTC). After comparing multiple sensors: including a standard 10 $k\Omega$ NTC thermistor and an LM34 temperature sensor, the precision thermistor was selected for its superior stability and accuracy when mounted on the panel. The thermistor is configured with a 10 $k\Omega$ resistor as a voltage divider, allowing temperature estimation via the Arduino's analog input.

The misting subsystem utilizes a low-side N-channel MOSFET to interface the Arduino with the high-current misting pump. An external 5 V supply was incorporated as a safety and reliability measure to ensure sufficient current delivery while electrically isolating the microcontroller. The MOSFET functions as a ground-side electronic switch, with the drain connected to the mister's negative terminal, the source to ground, and the gate driven through a series resistor by an Arduino digital output. Physical interfacing to the breadboard was achieved using a micro-USB cable and a female micro-USB–to-DIP 5-pin breakout board.

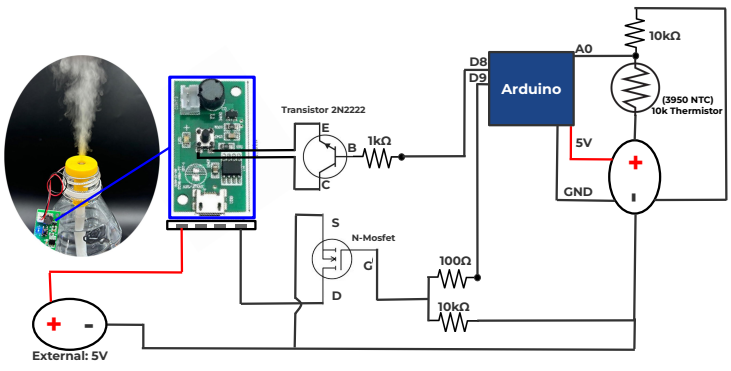

Figure 1: Schematic of Mister and Thermistor Wiring

2.1.1 Mister Manual Button Override System

An additional switch-like component, a transistor, was incorporated into the mister subsystem to provide electronic override of the manual push button on the circuit board. Because the mister's control board included a built-in manual push button, the MOSFET alone was insufficient to actuate the mister electronically. To address this limitation, wires were soldered across the terminals of the push button and connected to the transistor's collector and emitter, allowing the transistor to function as an electronically controlled switch. This configuration enables the Arduino to simulate a button press and override manual operation, as shown in Figure 2.

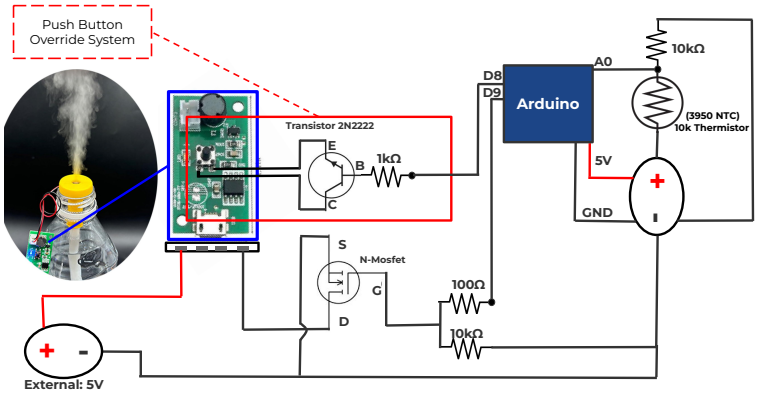

Figure 2: Schematic of Highlighted Wiring of Push Button Override

2.2 Solar Panel Power System

Power output from the solar panel was initially obtained using an INA219 power monitoring module (see Section 2.4). However, due to integration challenges, the system was reconfigured to use a voltage divider–based measurement approach. A known 220 Ω resistive load was combined with a symmetric voltage divider consisting of two 100 $k\Omega$ resistors, which is shown in Figure 3. This enabled a safe voltage acquisition and power calculation. A USB waterproof mini solar panel was used as the power source, and a USB male–to–4-pin female 28 AWG extender cable was employed to connect the panel output to the voltage divider measurement circuit.

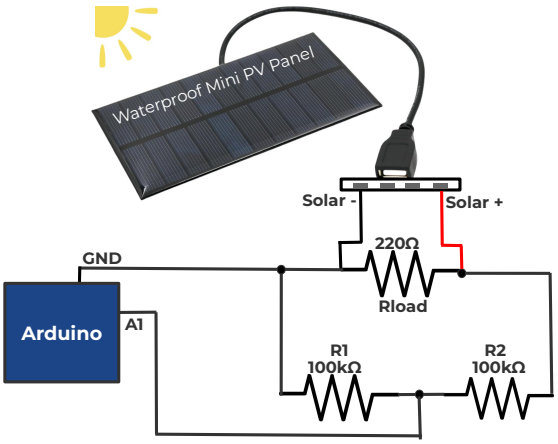

Figure 3: Schematic of Solar Panel Power Output Measurement

2.2.1 Voltage Divider Math

$$V_{\text{out}} = V_{\text{in}} \frac{R_2}{R_1 + R_2}$$

$$V_{\text{out}} = V_{\text{panel}} \frac{100\,\text{k}\Omega}{100\,\text{k}\Omega + 100\,\text{k}\Omega} = \frac{1}{2} V_{\text{panel}}$$

$$V_{\text{panel}} = 2V_{\text{out}}$$

$$I = \frac{V_{\text{panel}}}{R_{\text{load}}}$$

$$P = V_{\text{panel}} I$$

$$P = \frac{V_{\text{panel}}^2}{R_{\text{load}}}$$

2.3 Solar Replication System

To approximate real-world solar operating conditions in a laboratory environment, artificial illumination was used to replicate both the thermal and spectral components of solar irradiance. As illustrated in Figure 4, a halogen lamp was employed to induce panel heating, while 4 high-power growth lights provided consistent irradiance for photovoltaic power generation. This dual-source approach enabled controlled and repeatable testing of thermal effects on panel performance.

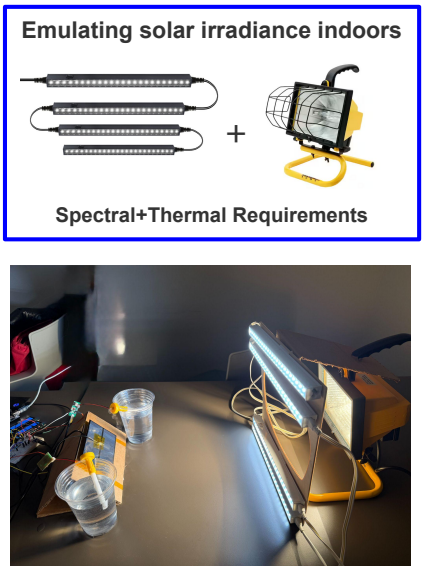

Figure 4: Artificial light system simulating solar power

2.4 I2C Communication

I²C communication was explored in two distinct ways within the system. The first implementation utilized a 16×2 LCD display with an I²C interface to present real-time system information, including thermistor temperature, mister on/off state, and the voltage and power output of the solar panel. The I²C protocol enables serial communication using two lines: SDA, a bidirectional data line used to transmit commands and display data, and SCL, the clock signal generated by the Arduino to synchronize data transfer on the SDA line.

A second I²C-based component, the INA219 power monitoring module, was intended for use in measuring the solar panel's electrical output. However, due to receiving a defective module and subsequent time constraints, this approach was replaced with a voltage divider–based measurement method. Under normal operation, the INA219 communicates with the microcontroller via the SDA and SCL lines and provides direct digital measurements of voltage, current, and power. Compared to a voltage divider, the INA219 offers improved measurement accuracy, enhanced functionality, and greater system reliability. Both systems are display in Figure 5.

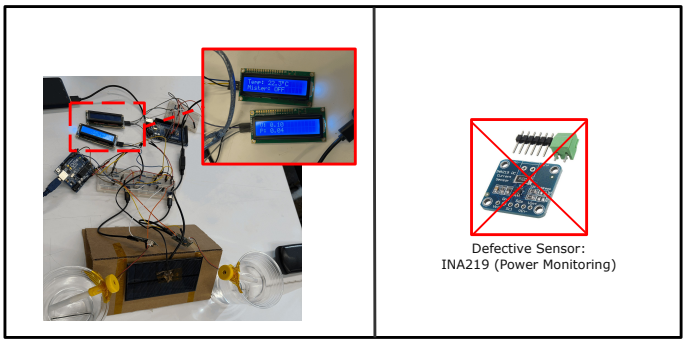

Figure 5: Systems with I2C Communication Abilities

3 Methodology

3.1 System Modeling

To build the system block diagram in Simulink, mathematical models were derived for all components of the system. As a first step, the transfer function of the solar panel (the plant) was obtained using the Energy Balance Equation.

3.2 Solar Panel Modeling (Plant):

The solar panel is modeled as a lumped thermal system with uniform temperature.

Definitions

$T(t)$: panel temperature
T_a: ambient temperature
m: effective mass
c_p: specific heat capacity

The thermal capacitance is defined as

$$C_{th} = mc_p \tag{1}$$

The heat input to the system is denoted by

$$Q_{in}(t) \tag{2}$$

Stored Thermal Energy

The thermal energy stored in the panel is

$$E(t) = mc_p T(t) \tag{3}$$

Taking the time derivative,

$$\frac{dE(t)}{dt} = mc_p \frac{dT(t)}{dt} = C_{th} \frac{dT(t)}{dt} \tag{4}$$

Heat Loss to Ambient

Heat transfer to the ambient is modeled using Newton's law of cooling:

$$Q_{loss}(t) = hA\left(T(t) - T_a\right) \tag{5}$$

The thermal resistance is defined as

$$R_{th} = \frac{1}{hA} \tag{6}$$

Thus, the heat loss term becomes

$$Q_{loss}(t) = \frac{T(t) - T_a}{R_{th}} \tag{7}$$

Energy Balance

From conservation of energy,

$$C_{th} \frac{dT(t)}{dt} = Q_{in}(t) - \frac{T(t) - T_a}{R_{th}} \tag{8}$$

Deviation Variable

Define the temperature deviation from ambient as

$$\theta(t) = T(t) - T_a \tag{9}$$

Substituting into the energy balance equation,

$$C_{th} \frac{d\theta(t)}{dt} = Q_{in}(t) - \frac{\theta(t)}{R_{th}} \tag{10}$$

Rearranging,

$$\frac{d\theta(t)}{dt} + \frac{1}{R_{th}C_{th}}\theta(t) = \frac{1}{C_{th}} Q_{in}(t) \tag{11}$$

Transfer Function

Taking the Laplace transform with zero initial conditions,

$$s\Theta(s) + \frac{1}{R_{th}C_{th}}\Theta(s) = \frac{1}{C_{th}} Q_{in}(s) \tag{12}$$

Factoring $\Theta(s)$,

$$\Theta(s)\left(s + \frac{1}{R_{th}C_{th}}\right) = \frac{1}{C_{th}} Q_{in}(s) \tag{13}$$

The transfer function from heat input to temperature rise is

$$\frac{\Theta(s)}{Q_{in}(s)} = \frac{\frac{1}{C_{th}}}{s + \frac{1}{R_{th}C_{th}}} \tag{14}$$

Multiplying numerator and denominator by $R_{th}C_{th}$,

$$\frac{\Theta(s)}{Q_{in}(s)} = \frac{R_{th}}{R_{th}C_{th}s + 1} \tag{15}$$

Final Plant Form

Define

$$K_{plant} = R_{th} \tag{16}$$

$$\tau_{plant} = R_{th}C_{th} \tag{17}$$

The resulting first-order thermal plant model is

$$\boxed{G_{plant}(s) = \frac{K_{plant}}{\tau_{plant}s + 1}} \tag{18}$$

3.3 Actuator Modeling (Mister)

To represent the ultrasonic mister in the Simulink block diagram, a dynamic model is required. Due to electrical, mechanical, and fluid-related delays, the mister does not respond instantaneously. Therefore, the actuator is modeled as a first-order system.

Definitions

$u(t)$: actuator input signal (PWM duty cycle or ON/OFF command)
$q_m(t)$: effective mist output (spray intensity)
K_{act} : actuator steady-state gain
τ_{act} : actuator time constant

Dynamic model

The mist output increases with the input command and naturally decays when the input is removed. Assuming linear behavior, the actuator dynamics can be described by the following balance equation:

$$\frac{dq_m(t)}{dt} = \alpha\, u(t) - \beta\, q_m(t) \tag{19}$$

Rearranging,

$$\frac{dq_m(t)}{dt} + \beta\, q_m(t) = \alpha\, u(t) \tag{20}$$

Define the actuator parameters as

$$\tau_{act} = \frac{1}{\beta}, \qquad K_{act} = \frac{\alpha}{\beta} \tag{21}$$

Substituting these definitions yields the standard first-order form:

$$\tau_{act}\frac{dq_m(t)}{dt} + q_m(t) = K_{act}\, u(t) \tag{22}$$

Transfer function

Taking the Laplace transform with zero initial conditions,

$$\tau_{act} s Q_m(s) + Q_m(s) = K_{act} U(s) \tag{23}$$

Thus, the actuator transfer function is

$$\boxed{G_{act}(s) = \frac{Q_m(s)}{U(s)} = \frac{K_{act}}{\tau_{act} s + 1}} \tag{24}$$

3.4 Sensor Modeling (NTC Thermistor)

The thermistor is mounted on the top surface of the PV panel. Due to its finite thermal mass and the thermal contact resistance to the panel, the measured temperature cannot change instantaneously. Therefore, the sensor is modeled as a first-order system from the panel surface temperature to the measured temperature.

Thermal balance

Let $T_p(t)$ be the PV surface temperature and $T_s(t)$ be the thermistor temperature (measured output). The thermistor is modeled as a lumped thermal mass with thermal capacitance C_s and thermal resistance to the panel R_{sp}.

Heat flow from the panel to the sensor:

$$Q(t) = \frac{T_p(t) - T_s(t)}{R_{sp}} \tag{25}$$

Energy balance on the thermistor:

$$C_s \frac{dT_s(t)}{dt} = Q(t) \tag{26}$$

Substitute $Q(t)$:

$$C_s \frac{dT_s(t)}{dt} = \frac{T_p(t) - T_s(t)}{R_{sp}} \tag{27}$$

Rearrange:

$$R_{sp}C_s \frac{dT_s(t)}{dt} + T_s(t) = T_p(t) \tag{28}$$

Define the sensor time constant:

$$\tau_{sensor} = R_{sp}C_s \tag{29}$$

Thus, the first-order sensor model is:

$$\tau_{sensor} \frac{dT_s(t)}{dt} + T_s(t) = T_p(t) \tag{30}$$

Transfer function

Taking the Laplace transform (zero initial conditions):

$$(\tau_{sensor}s + 1)T_s(s) = T_p(s) \tag{31}$$

Therefore,

$$\boxed{G_{sensor}(s) = \frac{T_s(s)}{T_p(s)} = \frac{1}{\tau_{sensor}s + 1}} \tag{32}$$

3.5 Parameter Settings

The system parameters were obtained experimentally by running the complete setup under heating and cooling conditions. The thermal response of the PV panel, actuator, and sensor was observed using step-like inputs and natural transients. Time constants were estimated from the dominant rise and decay times, while steady-state gains were inferred from the measured temperature changes. All components were then represented using effective first-order dynamics for control-oriented modeling.

Table 1: System Parameters

Block	**Parameter**	**Meaning**	**Value**
Actuator	$K_{actuator}$	Cooling gain from mister	-1400
Actuator	$\tau_{actuator}$	Pump / mister response time	5 s
Plant	K_{plant}	Cooling effectiveness (normalized)	0.025
Plant	τ_{plant}	Panel thermal time constant	400 s
Sensor	τ_{sensor}	Thermistor thermal lag	2 s
Environment	$T_{ambient}$	Ambient air temperature	26°C
Reference	T_{target}	Target panel temperature	41°C
Supervisory Logic	T_{high}	High-temperature threshold	44°C

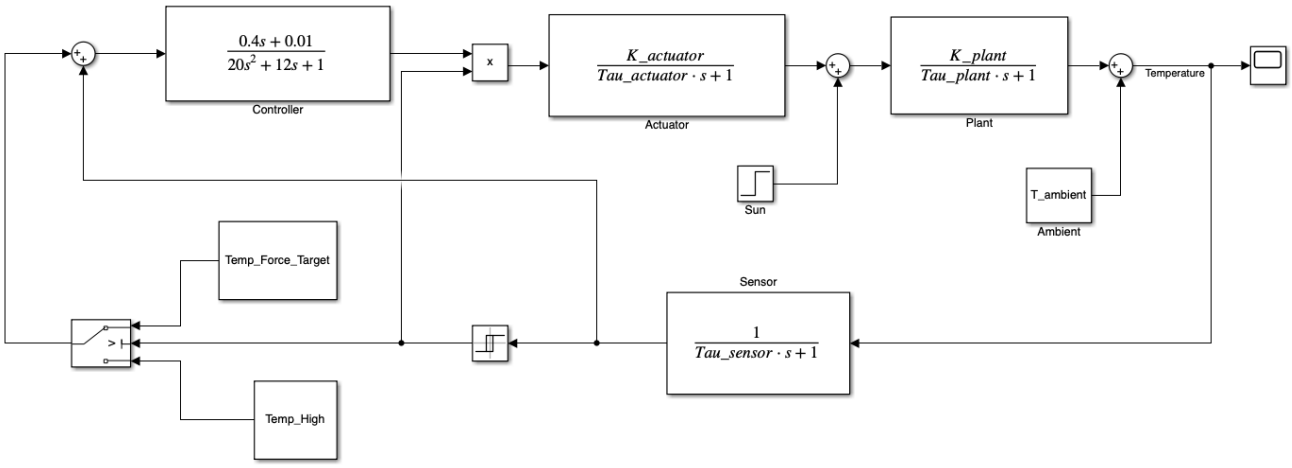

Figure 6: Block Diagram of the System

As shown in Figure 6, the actuator, plant, and sensor are connected. To model plant heating, a solar irradiance of 800 W/m² was applied to the system and an ambient temperature of 26 °C was included in plant output to ensure accurate modeling.

3.6 Controller Design

Since the plant has slow dynamics, a slow controller was selected to match the behavior of the system. The controller is second order with real and negative poles, ensuring a stable and non-oscillatory response. The poles are located at -0.01 and -0.05, while a zero at -0.025 is used to shape the response. This design choice is consistent with the slow nature of the plant.

$$C(s) = \frac{0.4s + 0.01}{20s^2 + 12s + 1} \tag{33}$$

Relay and switch blocks were also added in Simulink to implement the on–off logic of the cooling system. In the simulated solar panel cooling system, when the panel temperature reaches 44 °C, the controller and actuator are activated to cool the panel down to 41 °C, after which the system is turned off. The relay and switch blocks enable this temperature-based activation and deactivation behavior.

3.7 Calculation of the Closed-Loop Transfer Function

The closed loop system consists of the following components: Controller $C(s)$, Actuator $A(s)$, Plant $P(s)$, and Sensor $H(s)$. Their transfer functions are defined as:

$$\begin{aligned} C(s) &= \frac{0.4s + 0.01}{20s^2 + 12s + 1} \\ A(s) &= \frac{1400}{5s + 1} \\ P(s) &= \frac{0.025}{400s + 1} \\ H(s) &= \frac{1}{2s + 1} \end{aligned}$$

The Forward Path Transfer Function, $G(s) = C(s) \cdot A(s) \cdot P(s)$, is calculated as:

$$G(s) = \frac{14s + 0.35}{40000s^4 + 32100s^3 + 6880s^2 + 417s + 1} \tag{34}$$

The Closed-Loop Transfer Function $T(s)$ is derived using the standard feedback formula:

$$T(s) = \frac{G(s)}{1 + G(s)H(s)} \tag{35}$$

Substituting the values and simplifying the expression, the final closed-loop transfer function is obtained as:

$$T(s) = \frac{28s^2 + 14.7s + 0.35}{80000s^5 + 104200s^4 + 45860s^3 + 7714s^2 + 433s + 1.35} \tag{36}$$

Stability and Performance Analysis from Bode Plot

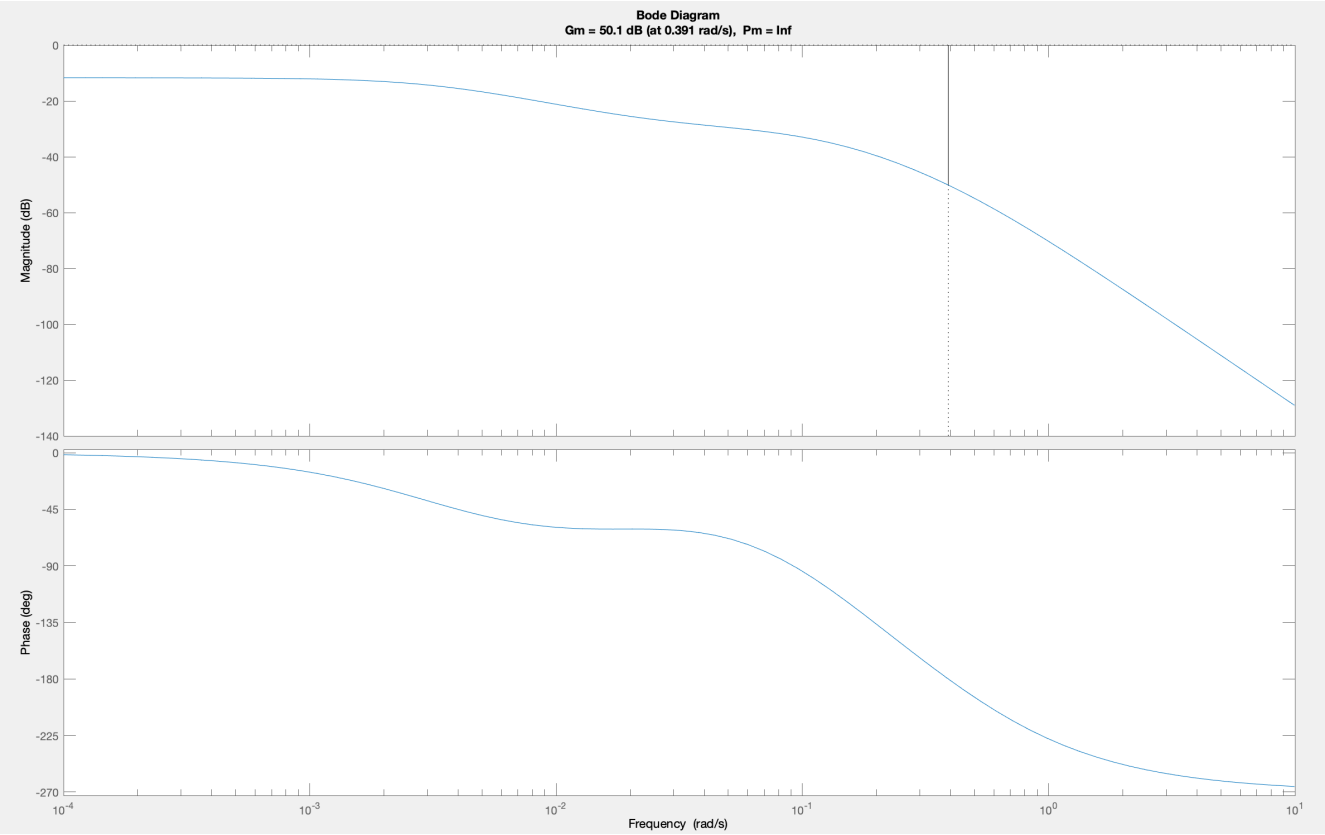

Figure 7: Bode Plot of the Closed-Loop System

The frequency response of the system was analyzed using the Bode diagram shown in Figure 7. The stability margins were calculated as follows:

- **Gain Margin (G_m):** 50.1 dB (at 0.391 rad/s)
- **Phase Margin (P_m):** Infinite (Inf)

Since the Gain Margin is positive ($G_m > 0$ dB), the closed-loop system is stable. The infinite Phase Margin indicates that the magnitude plot does not cross the 0 dB threshold, implying an unconditionally stable system with no phase crossover frequency issues in the current configuration.

3.8 Scopes of The Simulation

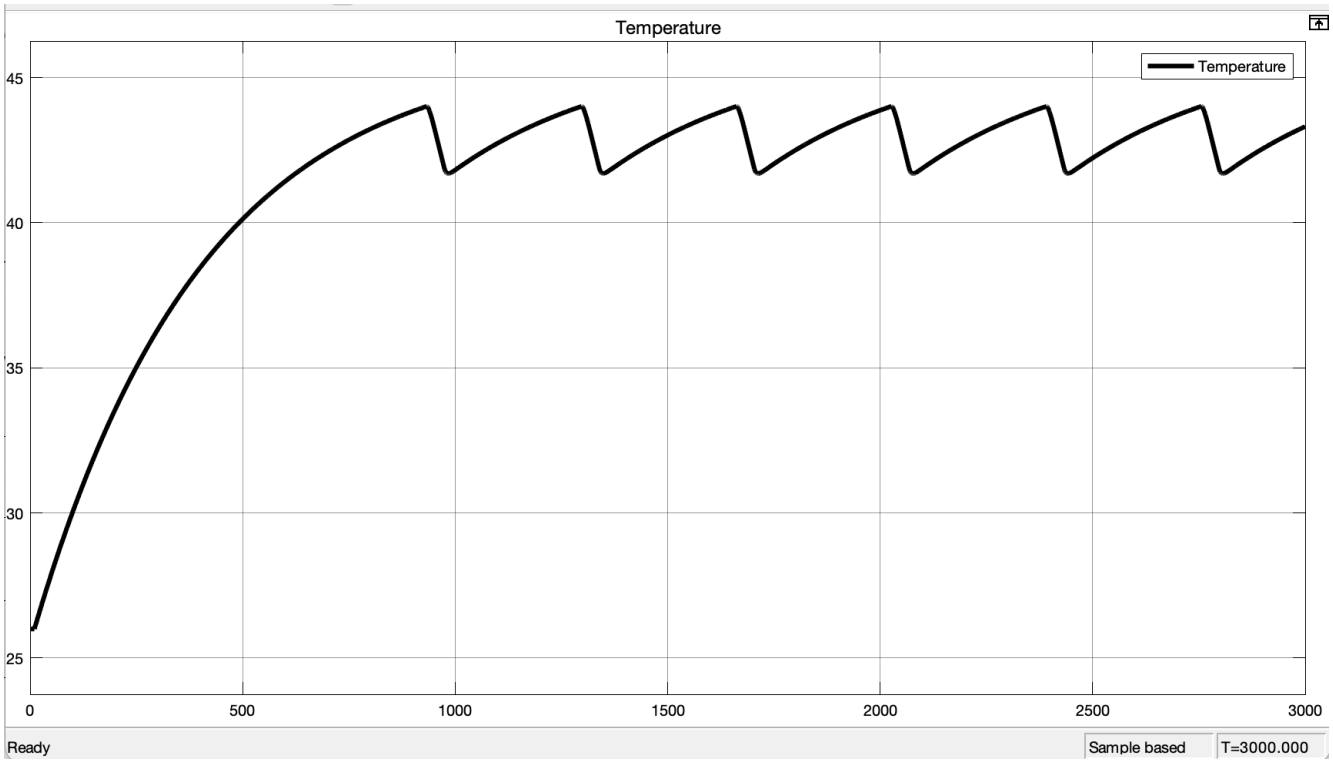

Figure 8: Temperature Scope of the Simulation

Simulation Results: Temperature Response

The time-domain response of the temperature control system is shown in the Figure 8. The simulation is run for 3000 seconds and the system behavior can be explained based on the relay switching logic.

The system starts from the ambient temperature of approximately 26°C and heats up gradually due to solar input. Because of the high thermal inertia of the panel, the temperature rises slowly and reaches the upper threshold after about 1000 seconds.

When the temperature reaches 44°C, the relay-based control logic activates the actuator. At this point, the controller enables the mister, and the cooling effect causes the panel temperature to decrease. The temperature is then reduced to 41°C, after which the actuator is switched off.

This ON OFF behavior repeats over time, resulting in a sawtooth-like temperature profile between 41°C and 44°C. This control strategy is intentionally designed to minimize water consumption by activating the mister only when necessary, rather than operating it continuously.

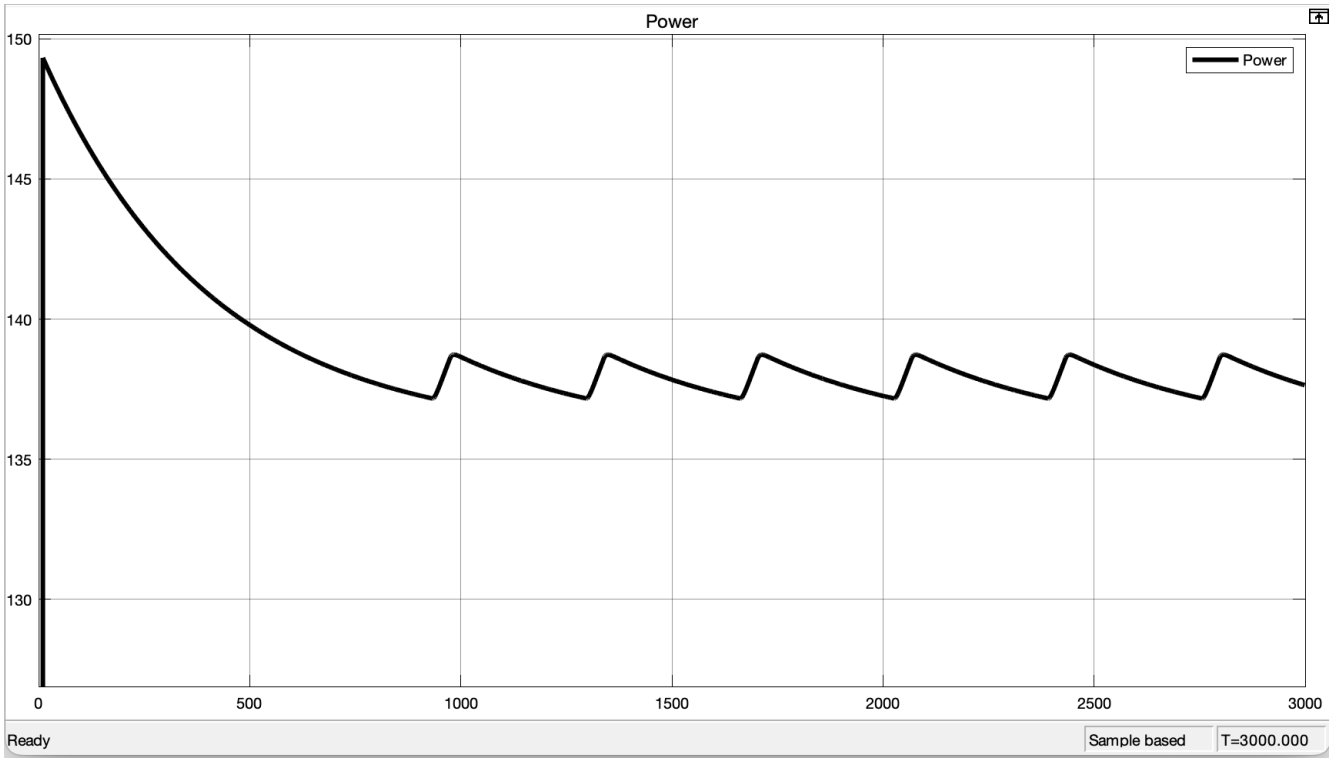

Figure 9: Power Output of the Simulation

Simulation Results: Power Output

The power output of the PV panel is shown in the Figure 9. As the panel temperature decreases due to the activation of the evaporative cooling system, the electrical power output increases.

During the initial heating phase, the power output gradually decreases as the panel temperature rises. Once the relay-based control logic activates the mister, the panel temperature is reduced, which leads to a noticeable recovery in power output. This behavior is observed as periodic increases in power that coincide with the cooling cycles.

The repeating pattern in the power signal directly reflects the ON OFF cooling strategy. Each cooling event improves panel efficiency by lowering the operating temperature, demonstrating the effectiveness of the proposed cooling approach in improving power output.

4 Software Architecture

4.1 Discrete Controller Implementation

The continuous controller was discretized using MATLAB and implemented on an Arduino microcontroller using a difference equation. The implementation closely follows the Simulink model and provides reliable control, monitoring, and communication for the experimental system.

The controller was first designed in continuous time using MATLAB. Designing the controller in continuous time makes tuning and analysis easier, especially for slow thermal systems. The continuous-time controller used in this project is given by

$$C(s) = \frac{0.4s + 0.01}{20s^2 + 12s + 1} \tag{37}$$

Since the controller is implemented on a microcontroller, it must operate in discrete time. For this reason, the continuous controller was discretized using the MATLAB `c2d` command. A sampling time of

$$T_s = 0.1 \text{ s} \tag{38}$$

was selected. This sampling time is fast enough to capture temperature changes while remaining suitable for real-time execution on the Arduino. The Tustin transformation was used for the discretization.

After discretization, the controller was expressed in the form of a difference equation suitable for real-time implementation. The discrete-time controller is given by

$$u[k] = b_0 e[k] + b_1 e[k-1] + b_2 e[k-2] - a_1 u[k-1] - a_2 u[k-2], \tag{39}$$

where $e[k]$ represents the control error and $u[k]$ represents the controller output. The numerical values of the coefficients obtained from MATLAB are

$$b_0 = 9.7197 \times 10^{-4}, \tag{40}$$

$$b_1 = 2.4269 \times 10^{-6}, \tag{41}$$

$$b_2 = -9.6954 \times 10^{-4}, \tag{42}$$

$$a_1 = -1.9413, \tag{43}$$

$$a_2 = 0.9418. \tag{44}$$

The control algorithm runs in a fixed-step loop with a sampling time of 0.1 seconds. At each step, the solar panel temperature is measured using an NTC thermistor. A relay block checks whether cooling is required. According to the relay state, the reference temperature is selected and the control error is calculated as

$$e[k] = T_{\text{ref}} - T[k]. \tag{45}$$

The discrete controller equation is then evaluated using the current and previous error values. The controller output is converted into an ON/OFF signal for the misting system. Since the actuator cannot receive a continuous control signal, a threshold is used to decide whether the misting system should be turned on or off.

Communication is used for monitoring and safe operation. Temperature and controller data are sent from the Arduino to a PC using serial communication in CSV format (comma-separated values). This allows offline analysis of the system behavior. The same serial interface is also used to stop the experiment when needed. In addition, an I2C LCD displays the current temperature, the selected reference, and the misting system status in real time. The display is updated at a low rate to avoid affecting the control loop.

5 Results

5.1 MATLAB-based live logging

This results below in Figure 10 and Figure 11 were produced through a MATLAB-based live logging and plotting script was used to capture data and communicate with the Arduino via serial interface to log temperature measurements and mister actuation state. Live visualization and automated CSV logging facilitate validation of control performance and quantitative analysis of the system's thermal response.

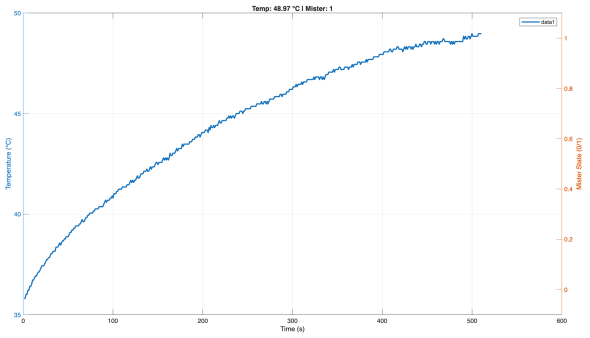

(a) Panel temperature response without evaporative cooling

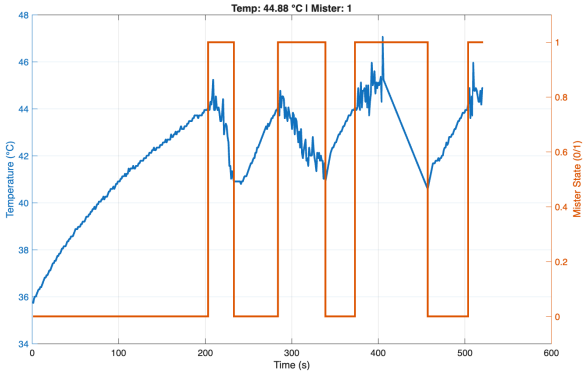

(b) Panel temperature response with mister control enabled

Figure 10: Comparison of solar panel temperature response under identical irradiance conditions. The uncontrolled case (left) exhibits continuous temperature rise, while the controlled case (right) demonstrates temperature regulation through evaporative misting.

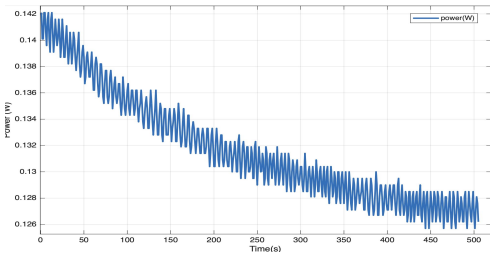

(a) Solar panel power output without evaporative cooling

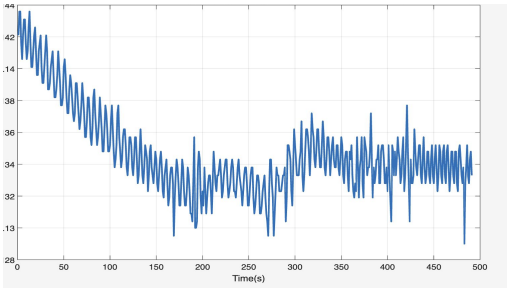

(b) Solar panel power output with mister control enabled

Figure 11: Comparison of solar panel power output under identical irradiance conditions. Without cooling (left), power output decreases steadily as panel temperature rises. With evaporative cooling enabled (right), power output degradation is reduced due to improved thermal regulation.

5.2 Temperature Regulation Performance

Experimental results show that evaporative cooling significantly alters the thermal behavior of the photovoltaic panel. In the uncontrolled case, the panel temperature increases monotonically under constant irradiance with no inherent stabilization. When closed-loop misting control is enabled, the panel temperature is successfully regulated between the predefined thresholds of 41 °C and 44 °C.

The relay-based control logic produces a repeatable ON OFF cooling pattern, resulting in a bounded, sawtooth like temperature profile. This behavior closely matches the simulated response and confirms that our thermal model captures the dominant system dynamics. The use of hysteresis prevents excessive actuator cycling and ensures stable operation.

5.3 Power Output Response

Measured power output exhibits a clear dependence on panel temperature. Without cooling, power output steadily decreases as the panel temperature rises. With evaporative cooling enabled, temperature-induced power degradation is reduced, and periodic recoveries in power output are observed during cooling cycles.

Although the absolute power gains are modest due to the small panel size and indoor testing conditions, the results validate the underlying principle that active thermal regulation can preserve photovoltaic efficiency. The observed trends are consistent with known temperature-efficiency relationships in photovoltaic systems.

5.4 Energy Considerations

At the scale of this experiment, the energy consumed by the misting system exceeds the additional electrical energy recovered through cooling. This outcome is expected due to scale mismatch, non-optimized mist delivery, and laboratory operating conditions. Nevertheless, the results demonstrate that the control strategy itself is effective, independent of overall energy balance at small scale.

6 Key Limitations

Despite demonstrating effective temperature regulation and power stabilization, the proposed system has several limitations that constrain quantitative performance and generalizability.

6.1 Scale Mismatch

The experimental setup uses a small photovoltaic panel operating under indoor illumination. At this scale, the energy consumed by the misting actuator exceeds the electrical energy recovered through cooling. As a result, net energy efficiency cannot be meaningfully evaluated. These effects are expected to change at larger panel areas where thermal inertia and electrical output scale more favorably.

6.2 Indoor Irradiance Approximation

Solar irradiance was emulated using artificial light sources to independently reproduce thermal loading and electrical generation. While this approach enables repeatable testing, it does not fully capture the spectral distribution, spatial uniformity, or dynamic variability of natural sunlight. Consequently, absolute power values cannot be directly extrapolated to outdoor conditions.

6.3 Binary Actuation

The misting system operates using on off control through relay logic rather than continuous modulation. This limits control resolution and results in a sawtooth temperature profile. Although effective for thermal regulation, this approach may not be optimal for minimizing water consumption or actuator wear.

6.4 Non-uniform Mist Distribution

The evaporative cooling effect is highly dependent on mist coverage and evaporation efficiency. In the current setup, mist distribution across the panel surface is nonuniform, leading to localized cooling rather than homogeneous temperature reduction. This limits overall cooling effectiveness and introduces spatial thermal gradients that are not captured by the model.

6.5 Measurement Accuracy

Electrical power output is estimated using a voltage divider and resistive load rather than a dedicated power monitoring device. This approach introduces uncertainty due to resistor tolerances, noise, and limited current resolution. Sensor placement and thermal contact resistance also affect temperature measurement accuracy.

6.6 Environmental Disturbance Exclusion

The model assumes constant ambient temperature and negligible wind effects. In real outdoor environments, convective heat transfer and environmental disturbances play a significant role in panel thermal behavior. The absence of these effects limits the applicability of the results to controlled laboratory conditions.

7 Conclusion

This project demonstrates the successful design, modeling, and implementation of a closed-loop evaporative cooling system for photovoltaic panels. A control-oriented framework was used to regulate panel temperature using real-time sensing and actuator feedback, supported by first-order dynamic models of the panel, actuator, and sensor. Simulation and experimental results show strong qualitative agreement, validating both the modeling assumptions and the controller design.

Controlled evaporative cooling was shown to reduce panel temperature and mitigate temperature-induced power losses compared to uncontrolled operation. While the system is not energy-positive at the tested scale, the results highlight the importance of intelligent control strategies over continuous or open-loop cooling approaches.

The primary contribution of this work lies in framing photovoltaic cooling as a dynamic systems and control problem supported by experimental validation. The architecture and modeling framework developed in this project provide a foundation for higher-fidelity implementations, improved actuator efficiency, and scalable designs suitable for real-world photovoltaic systems.

8 Future Steps

Several improvements can be made to increase the fidelity, efficiency, and scalability of the proposed photovoltaic cooling system.

8.1 High-Fidelity System Architecture

Future work will extend the current SISO framework to an MIMO system. Additional control inputs may include mist pulse frequency, backside airflow velocity, and coolant temperature for liquid-based cooling. Additional outputs such as water consumption, cooling efficiency, and actuator duty cycle would enable more comprehensive performance evaluation and optimization.

8.2 Environmental Disturbance Modeling

The current model assumes constant ambient conditions. Future implementations should incorporate environmental disturbances such as ambient temperature variation, wind speed, and convective heat transfer changes. Including these disturbances would improve model accuracy and allow the controller to adapt to realistic outdoor operating conditions.

8.3 Alternative Cooling Modalities

Beyond evaporative misting, alternative cooling approaches can be explored. These include pneumatic airflow systems for convective enhancement, backside liquid cooling channels, and hybrid systems combining misting and forced airflow. Comparative evaluation of these methods would help identify cooling strategies that maximize heat removal while minimizing energy and water usage.

8.4 Scaling and Field Deployment

The system should be scaled to larger panel areas or multi-panel arrays to evaluate whether temperature regulation produces net positive energy gains at realistic operating scales. Long-duration outdoor testing under natural irradiance cycles would enable validation of thermal performance, robustness, and reliability. Field deployment would also require weatherproof packaging, autonomous scheduling, and safety interlocks.

8.5 Measurement and Sensing Improvements

Future iterations should replace voltage divider based power estimation with dedicated power monitoring hardware such as an INA219 or equivalent sensor. Improved sensor placement and additional temperature measurements across the panel surface would allow spatial thermal gradients to be captured and modeled more accurately.

8.6 Control Strategy Enhancements

More advanced control strategies such as model predictive control or adaptive control could be implemented to reduce actuator usage while maintaining thermal regulation. These approaches would allow the system to anticipate thermal loading and optimize cooling behavior under changing environmental conditions.

References

[1] "Maximizing solar photovoltaic efficiency with mist cooling," *Energy Conversion and Management*, 2025. Available: https://www.sciencedirect.com/science/article/pii/S0196890425003887

[2] "Overview of recent solar photovoltaic cooling systems," *Inventions*, MDPI, vol. 12, no. 9, 2024. Available: https://www.mdpi.com/2227-7080/12/9/171

[3] "Performance investigation of solar photovoltaic panels with mist cooling," *Energy Sources, Part A: Recovery, Utilization, and Environmental Effects*, 2024. Available: https://www.tandfonline.com/doi/full/10.1080/15567036.2024.2305302

[4] "Enhancing the efficiency of solar panel using cooling systems," review paper, ResearchGate. Available: https://www.researchgate.net/publication/315996003